OXYGEN ISOTOPIC HETEROGENEITY IN AN ULTRAREFRACTORY PHASE BEARING CAI FROM A REDUCED TYPE CV3 CHONDRITE RBT 04143. T. Yoshizaki[1], D. Nakashima[1], T. Nakamura[1], C. Park[2], N. Sakamoto[3], H. Ishida[1], and J. I. Lee[2], [1]Division of Earth and Planetary Materials Science, Tohoku University, Sendai, Miyagi 980-8578, Japan (tacasy22@dc.tohoku.ac.jp); [2]Division of Earth-System Sciences, Korea Polar Research Institute, Incheon 21990, South Korea; [3]Isotope Imaging Laboratory, Creative Research Institution Sousei, Hokkaido University, Sapporo 001-0021, Japan.

Introduction: Calcium-aluminum-rich inclusions (CAIs) are thought to be the oldest solids [e.g., 1] and the key to understanding of physicochemical conditions in the early Solar System. Ultrarefractory (UR) minerals enriched in Sc, Zr, and/or Y rarely occur both in the melted and unmelted CAIs, thought to have formed at higher temperature compared to normal CAI minerals (e.g., melilite, spinel and Al-Ti-diopside). Therefore, UR phases can potentially provide constraints on high temperature processes occurred in the nebula gas. However, it has not been well constrained whether UR minerals formed from a gas or a melt [e.g., 2, 3]. In addition, the origin of heterogeneous oxygen isotopic composition observed in some UR-phase-rich inclusions [e.g., 3, 4] is poorly understood.

Here we report petrology, mineral chemistry and oxygen isotopic compositions of the ultrarefractory phase bearing CAI R3C-01 from Roberts Massif (RBT) 04143 (CV_{red}; [5]).

Sample and Analytical Methods: Petrology and mineralogy of the CAI R3C-01 in a thin section of RBT 04143 was studied using FE-SEM at Tohoku University (TU). Quantitative X-ray microanalyses of CAI minerals and X-ray elemental mapping were performed at TU and Korea Polar Research Institute with FE-EPMAs using WDS detectors. Grain boundaries of minerals were determined by crystal orientation mapping with EBSD system equipped with the TU FE-SEM. Oxygen isotopic compositions of individual minerals and quantitative oxygen isotope images (isotopographs) in R3C-01 were obtained with the isotope microscope system at Hokkaido University, consisting of the Cameca ims-1270 and SCAPS ion imager. Analytical conditions are similar to those in [6].

Results: Ultrarefractory phase bearing CAI R3C-01 is an irregular-shaped, compound inclusion that consists of five lithological units. All units consist of melilite, spinel, perovskite and Al-Ti-rich pyroxene with various modal abundances. Outer margin of the inclusion is surrounded by Wark-Lovering (WL) rim and forsteritic (mostly $Fa_{<1}$) olivine rim. Some olivine grains from the outermost part of the rim have low-iron, manganese-enriched (LIME) compositions. R3C-01-u1 is the largest unit of R3C-01, consisting of fine (< 50 μm) grains of melilite, spinel, minor perovskite, Al-Ti-rich pyroxene (Figs. 1 and 2), and refractory metal nuggets (not shown). Anorthite replacing melilite as thin layers (< 10 μm) at some boundaries between WL rim and the outer margin of R3C-01-u1 is the only secondary phase in this inclusion. Other secondary phases such as nepheline, sodalite and hydrous silicates are not observed. Some spinel grains form framboids enclosing melilite (Fig. 1). Chemical compositions of spinel and perovskite in R3C-01-u1 are similar to those in normal refractory inclusions [e.g., 7]. Reversely-zoned, Åk-rich melilite (typically $Åk_{15\text{-}20}$ in the core and $Åk_5$ at the rim) and unzoned Åk-poor melilite (typically $Åk_5$) are heterogeneously distributed in the inclusion (Fig. 2). Most Al-Ti-rich pyroxenes in R3C-01-u1 are adjacent to perovskite and/or spinel. They are Sc-poor, Al-Ti-rich diopside (grossmanite ($CaTi^{3+}AlSiO_6$) [8] and kushiroite ($CaAlAlSiO_6$) [9]) with 0.1-0.5 wt% Sc_2O_3 and 0.2-1.4 wt% V_2O_3. On the other hand, some Al-Ti-rich pyroxene grains isolated in reversely-zoned melilite are Ti-V-rich davisite ($CaScAlSiO_6$) [10], highly enriched in Sc and V (6.2-8.9 wt% Sc_2O_3 and 2.2-3.7 wt% V_2O_3). Ti-V-rich davisite were not observed in other units of R3C-01.

Oxygen isotopographs of R3C-01-u1 minerals show that the CAI is mostly composed of two isotopically distinct regions: ^{16}O-poor ($-20 \leq \delta^{18}O \leq 0‰$) region that consists of reversely-zoned melilite ($Åk_{15\text{-}20}$ at core to $Åk_5$ at rim) and Ti-V-rich davisite; and ^{16}O-rich ($-50 \leq \delta^{18}O \leq -40‰$) region that consists of unzoned, gehlenitic melilite ($Åk_5$), Al-Ti-rich diopside and spinel (Fig. 2). The $\delta^{18}O$ values change sharply at the grain boundaries between ^{16}O-rich and ^{16}O-poor melilites. These two chemically and isotopically distinct regions distribute randomly in this inclusion.

Discussion: Heterogeneous distribution of oxygen isotopic compositions have been often observed in coarse-grained CAIs from CV3 chondrites and FGIs from higher petrologic type chondrites [11; references therein]. Such oxygen isotopic heterogeneities are considered to be resulted from isotope exchange with ^{16}O-poor gas during nebular reheating processes and/or with ^{16}O-poor fluid during fluid-assisted thermal metamorphism on the chondrite parent bodies [e.g., 11].

Sharp changes of $\delta^{18}O$ values at grain boundaries (Fig. 2) suggest that this inclusion have never experienced partial melting that could result in oxygen isotope variation within a single crystal [12]. Presence of

reversely zoned melilite, that cannot be explained by crystallization from a melt [13], is also inconsistent with partial melting. This inclusion may have escaped from parent body alteration, given (1) the lack of alteration products including alkali- and/or iron-bearing phases [e.g., 14] and (2) presence of LIME olivine, which is easily lost during parent body metamorphism [15]. In addition, oxygen isotope compositions of melilite do not correlate with the distance from the outer margin of the inclusion as reported in some CV CGIs [16, 17]. The random distribution of ^{16}O-rich regions and ^{16}O-poor regions and abrupt changes of δ^{18}O values at the grain boundaries in the CAI are inconsistent with gas-solid exchange and subsequent diffusion of oxygen isotopes during nebular reheating events [16, 17]. Therefore, it is suggested that oxygen isotopic compositions of minerals in the CAI have never been modified by these processes.

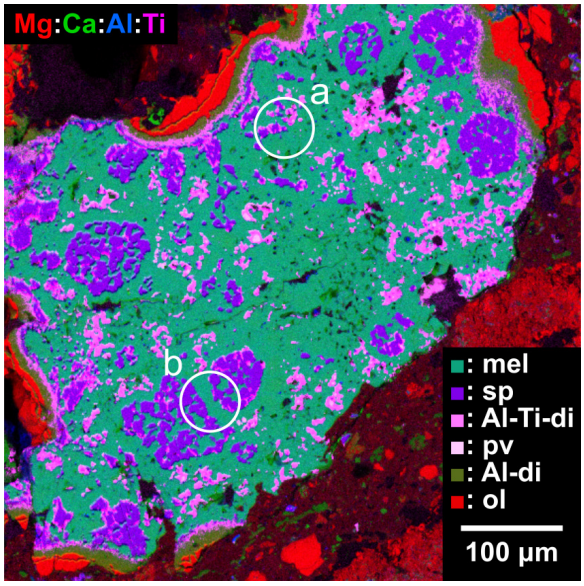

Fig. 1. Combined elemental map in Mg (red), Ca (green), Al (blue) and Ti (pink) K_α X-rays image of R3C-01-u1. The analysis areas for isotopography (Fig. 2) are also shown by white circles.

We argue that isotopically and mineralogically distinct two regions in R3C-01-u1 have condensed separately from different gaseous reservoirs, and subsequently aggregated to form the inclusion. Occurrence of ^{16}O-poor Ti-V-rich davisite in ^{16}O-poor reversely-zoned melilite suggests that Ti-V-rich davisite condensed prior to condensation of reversely-zoned melilite from ^{16}O-poor nebular gas. Alternatively, Ti-V-rich davisite could be relict that originated from an UR or normal CAI [18]. However, lack of other possible ^{16}O-depleted relict grains in R3C-01-u1 and absence of davisite with similar chemical composition in previously-studied inclusions might be inconsistent with this scenario. In any cases, it is suggested that spatially and/or temporally distinct ^{16}O-rich and ^{16}O-poor gaseous reservoir may have existed in the period of CAIs and UR phase formation.

References: [1] Connelly J.N. et al. (2012) *Science*, *338*, 651-655. [2] El Goresy A. et al. (2002) *GCA*, *66*, 1459-1491. [3] Ivanova M.A. et al. (2012) *MAPS*, *47*, 2107-2127. [4] Aléon J. et al. (2010) *MAPS*, *73*, Abstract#5185. [5] Ishida et al. (2012) *Polar Sci.*, *6*, 252-262. [6] Park C. et al. (2012) *MAPS*, *47*, 2070-2083. [7] Brearley A.J. and Jones R.H. (1998), *Rev. Mineral. Geochem.*, 36, 3.1-3.398. [8] Ma C. and Rossman G.R. (2009) *AM*, *94*, 1491-1494. [9] Kimura M. et al. (2009) *AM*, *94*, 1479-1482. [10] Ma C. and Rossman G.R. (2009) *AM*, *94*, 845-848. [11] Yurimoto H. et al. (2008) *Rev. Mineral. Geochem.*, *68*, 141-186. [12] Yurimoto H. et al. (1998) *Science*, *282*, 1874-1877. [13] MacPherson G.J. and Grossman L. (1984) *GCA*, *48*, 29-46. [14] Krot A.N. et al. (1998) *MAPS*, *33*, 1065-1085. [15] Komatsu M. et al. (2015) *MAPS*, *50*, 1271-1294. [16] Simon J.I. et al. (2011) *Science*, *331*, 1175-1178. [17] Simon J.I. et al. (2016) *GCA*, *186*, 242-276. [18] Lin Y. et al. (2003) *MAPS*, *38*, 407-417.

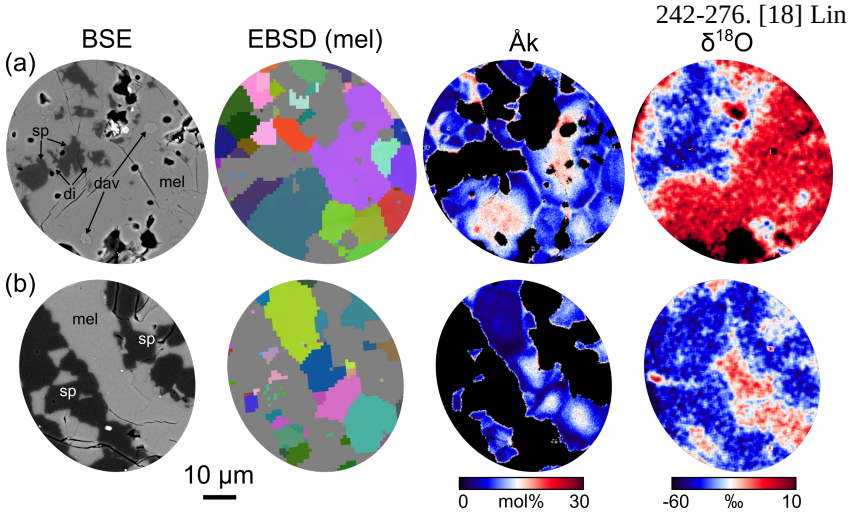

Fig. 2. BSE image, EBSD crystal orientation map of melilite, Åk content map of melilite and δ^{18}O isotopograph. Dav = Ti-V-rich davisite; di = Al-Ti-rich diopside; mel = melilite; sp = spinel.